
Article:
Amphlett, J.T.M., Pepper, S.E., Riley, A.L. orcid.org/0000-0001-5086-6636 et al. (5 more authors) (2020) Impact of copper(II) on activation product removal from reactor decommissioning effluents in South Korea. Journal of Industrial and Engineering Chemistry, 82. pp. 261-268. ISSN 1226-086X

https://doi.org/10.1016/j.jiec.2019.10.022

Impact of Copper(II) on Activation Product Removal from Reactor Decommissioning Effluents in South Korea

J. T. M. Amphlett[1,2*], S. E. Pepper[1], A. L. Riley[1], L. M. Harwood[3], J. Cowell[3], K. R. Whittle[4], T. S. Lee[5], and M. D. Ogden[1]

[1]*Separations and Nuclear Chemical Engineering Research (SNUCER), Department of Chemical and Biological Engineering, University of Sheffield, Sheffield, United Kingdom*
[2]*Nuclear and Quantum Engineering Department, Korea Advanced Institute of Science and Technology (KAIST), Daejeon, South Korea*
[3]*Department of Chemistry, University of Reading, Reading, United Kingdom*
[4]*School of Engineering, University of Liverpool, Liverpool, United Kingdom*
[5]*Department of Organic Materials Engineering, Chungnam National University, Daejeon, South Korea*

*j.amphlett@kaist.ac.kr

Keywords: Ion Exchange, Copper, Nickel, Cobalt, Functionalised Silica, Nuclear Decommissioning

Abstract

Decommissioning is one of the most important phases in the life of a nuclear reactor, having a major influence on public perception of such technology. Therefore, development of technologies that make decommissioning more safe, effective and efficient is integral to the success of the nuclear industry. In this paper, phosphonic acid functionalised silica has been studied to determine its suitability for treating nuclear decommissioning effluents produced in the HYBRID process, developed in South Korea. Cu^{2+} recovery from HCl media in both static and dynamic modes was investigated, as well as the effect of Cu^{2+} on Co^{2+} and Ni^{2+} recovery in a column loading system. Isothermal loading studies predicted a maximum loading capacity for Cu^{2+} of 22.82 mg g^{-1}, however complex loading behaviour was observed. Cu^{2+} sorption followed pseudo-second order kinetics with rapid uptake. Thermodynamic parameters have been extracted from collected kinetic data. Cu^{2+} outcompetes both Co^{2+} and Ni^{2+} for binding to the silica in column studies, which has implications for the use of phosphonic acid functionalised silica in treating decommissioning effluents. This work presents initial lab scale experiments, but shows the potential of Si based extractants for use in metals recovery in the nuclear industry.

1. Introduction

South Korea has undergone rapid civil nuclear expansion since 1961, with 24 reactors currently in operation, comprising 25.5% of its total energy generation [1,2]. With nuclear power producing 10% of total electricity globally, these figures illustrate South Korea's above average reliance on nuclear, making it the 5th largest producer of electrical energy from nuclear in the world [1]. However, a recent change in president has brought about a shift in Korean civil nuclear policy, whereby nuclear power will be phased out over roughly the next 45 years in favour of renewables and natural gas [3,4]. This nuclear phase out not only presents a complex decommissioning challenge, but

also an opportunity to grow world leading expertise in pressurised water reactor (PWR) decommissioning strategies. As of 2018, the only Korean reactor to have been shut down is the Kori-1 reactor, with decommissioning expected to begin in 2022 [4]. This decommissioning target has increased research activity in this area, particularly at the Korea Hydro & Nuclear Power (KHNP) Central Research Institute, and the Korea Atomic Energy Research Institute (KAERI).

Steel is a major component in nuclear reactors, and will have become contaminated with radionuclides throughout the life of the reactor. As the disposal of radioactive waste is expensive (£9630 m^{-3} in the UK, $12,500 per 200 L drum in Korea, for example), a process whereby the volume of steel for disposal as radioactive waste is minimised must be employed [5,6]. There have been a variety of steel decontamination methods researched and implemented throughout the history of nuclear power, including reductive processes such as CITROX, CAN-DEREM, LOMI and CORD, and oxidative processes involving permanganate [7,8]. These processes involve the use of organic chelating ligands such as EDTA, oxalic acid and citric acid, which help stabilise contaminant radionuclides in solution, thus aiding in the decontamination process. However, these chelating ligands may also promote solubility of these radionuclides in a geological disposal facility (GDF) and promote their migration into the subsurface and biosphere. This has prompted a focus on developing a new decontamination process in Korea which does not use these ligands, the HYBRID process [7,9–11].

The HYBRID (hydrazine based reductive metal ion decontamination) process was developed at KAERI. It utilises a hydrazine-copper complex to catalytically reduce ferric to ferrous, promoting dissolution of the steel surface and decontamination of radioactive species (Eq. 1 – 3) [9]. The proposed process also includes an oxidation step using nitric permanganate (NP). This NP-HYBRID process has been successfully tested on contaminated steel from the fuel test loop (FTL) research reactor, with dose rate from the specimen dropping from 516 to 0.5 µSV hr^{-1} after two oxidation-reduction cycles [9]. It is likely that the resulting effluent will contain Cu^{2+}, Ni^{2+} and Co^{2+} from the decontamination process, which will need to be recovered from the decontamination circuit.

$$N_2H_4 + Cu^+ \rightarrow [Cu(N_2H_4)]^+ \quad \textbf{(1)}$$

$$2[Cu(N_2H_4)]^+ + 8HNO_3 + Fe_3O_4 \rightarrow 3Fe^{2+} + 2[Cu(N_2H_4)]^{2+} + 4H_2O + 8NO_3^- \quad \textbf{(2)}$$

$$2[Cu(N_2H_4)]^{2+} + \frac{1}{2}N_2H_4 \rightarrow 2[Cu(N_2H_4)]^+ + \frac{1}{2}N_2 + 2H^+ \quad \textbf{(3)}$$

In the nuclear industry the most commonly employed metal recovery methods are ion exchange (IX) and solvent extraction (SX) [12]. Both technologies have advantages depending on the flowsheet they are being applied too. For the process discussed in this work, IX was deemed more suitable than SX, due to the fact that it removes issues with third phase and problematic degradation product formation, does not involving the use of large volumes of flammable and/or toxic organic solvents, and can more effectively recover metals at low concentration, amongst others [13].

IX extractants can be thought of as being composed of a molecular functional group, responsible for extracting solutes from the solvent, covalently bonded to an inert backbone matrix. The choice of functional group and matrix will primarily be dependent on the solution conditions of

the process, as well as other engineering concerns such as final waste disposal, an important factor in the nuclear fuel cycle. There are many options for matrix structure, including synthetic polymers, biopolymers, and silica, to name a few [14–20]. This is also the case for the functional group, with a plethora of potential molecular functionalities that can be grafted onto solids for metal recovery purposes [21–24].

In this work we have chosen silica functionalised with ethyl/butyl phosphonic acid (EBP-Si; PhosphonicS PO1) (Figure 1). EBP-Si was chosen as it has shown remarkably fast uptake kinetics towards Co^{2+} and Ni^{2+} from aqueous solutions in previous work, and gives the possibility for direct conversion into a final nuclear industry compatible wasteform (glass or concrete) for disposal. The possibility of direct conversion to a wasteform has the potential to be incredibly impactful within the nuclear industry. It would reduce the complexity of wasteform production through removing the production of secondary wastes associated with stripping steps, and minimises hazards and difficulties associated with radioactive waste IX resins [18]. Additionally, the application of silica based extractants to actinide recovery provides further safeguards against proliferation, as they would be converted directly into a solid wasteform. This study builds on previous work looking at the suitability of EBP-Si for Co^{2+} and Ni^{2+} recovery from acidic nuclear decommissioning effluents [18]. The uptake behaviour of Cu^{2+} has been determined in both batch and column loading systems, as well as the effect of metal loading from mixed Cu^{2+}, Co^{2+} and Ni^{2+} acidic, aqueous systems.

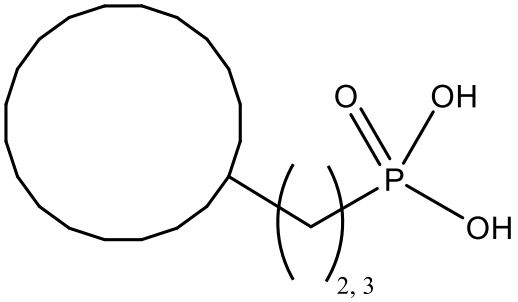

Figure 1. Structure of the functional group of EBP-Si.

2. Experimental

2.1 Equipment and reagents

Metal salts (98%+, $CuCl_2$, $CoCl_2$ and $NiCl_2$) and HCl (ACS reagent, 37%) were purchased from Sigma Aldrich and used as received. EBP-Si was purchased from PhosphonicS and preconditioned by contacting with HCl before use (1 M, 1:10 Vol:Vol ratio). Manufacturers technical data for EBP-Si can be found in Table 1. All solutions were made using deionised water (> 18 MΩ). Metal analysis was carried out in triplicate by atomic absorption spectroscopy (AAS) using a Perkin Elmer AAnalyst 400.

Table 1. Manufacturer's technical data for EBP-Si.

Functionality	Ethyl/butyl phosphonic acid
Product code	CP156871
Description	Non-porous functionalized silica
Appearance	White solid
H^+ capacity / mmol g^{-1}	0.9 – 1.2
Bulk Density / g L^{-1}	550 – 650
Hausner ratio	1.01 – 1.11
Particle size	95 % > 600 µm (100 % > 1200 µm)

2.2. Equilibrium Loading Studies

Equilibrium loading studies were performed to assess the effect of $[H^+]$ and $[Cu^{2+}]$ on Cu^{2+} sorption by EBP-Si. All equilibrium studies used 0.8 g of EBP-Si, which had been preconditioned as described in section 2.1. For the pH screening, EBP-Si was contacted with Cu^{2+} containing aqueous phases (30 mL, $[Cu^{2+}]$ 0.1 g L^{-1}, $[H^+]$ = 0.0001 – 1.2 M as HCl) and agitated on an orbital shaker (> 12 hours, 30 °C). Isotherm studies were performed by contacting EBP-Si with acidic, aqueous solutions containing varying $[Cu^{2+}]$ (30 mL, pH = 3, $[Cu^{2+}]$ = 25 – 2500 mg L^{-1}) and agitating on an orbital shaker (> 12 hours, 30 °C). Kinetic experiments were performed identically to the isotherm studies, but with a constant $[Cu^{2+}]$ (0.1 g L^{-1}) and varying contact time (30 – 600 s). Kinetic studies were performed at 30, 40, 50 and 60 °C.

2.3. Column Loading Studies

Column loading experiments were performed at varying influent flow rates (1 – 130 bed volumes (BV) hr^{-1}, 1 BV = 1.4 mL) in pH 3 HCl media. Experiments were performed from single and ternary metal aqueous phases. Single metal experiments had $[M^{2+}]$ = 0.1 g L^{-1}, and ternary metal experiments had $[M^{2+}]_{Total}$ = 0.1 g L^{-1}, with $[Cu^{2+}] = [Co^{2+}] = [Ni^{2+}]$.

3. Results and Discussion

3.1. Equilibrium Loading Studies

It was observed that increasing $[H^+]$ above 3 mM (pH 3) causes a reduction in Cu^{2+} extraction (Fig. 2). This is primarily due to the IX nature of Cu^{2+} recovery by EBP-Si, whereby two protons are exchanged for one Cu^{2+} ion. (Eq. 1). Effectively shifting the chemical equilibrium towards the phosphonate group remaining protonated, agreeing with pK_a values determined previously (pK_1 = 6.46, pK_2 = 6.38) [18]. This suggests that this system is suitable for effluents from the HYBRID process as it is operated between pH 2.5 and 3 [7]. The pH_{50} value for Cu^{2+} recovery is 1.12, estimated from polynomial fitting of the 5 closest data points to 50% Cu^{2+} extraction. This value is lower than that observed for Co^{2+} and Ni^{2+} in previous work (1.21 and 1.41, respectively) [18]. This suggests that Cu^{2+} has a stronger interaction with the EBP-Si than Co^{2+} and Ni^{2+}, and may therefore outcompete them for binding.

$$LH_2 + Cu^{2+} \rightleftharpoons LCu + 2H^+ \quad \textbf{(1)}$$

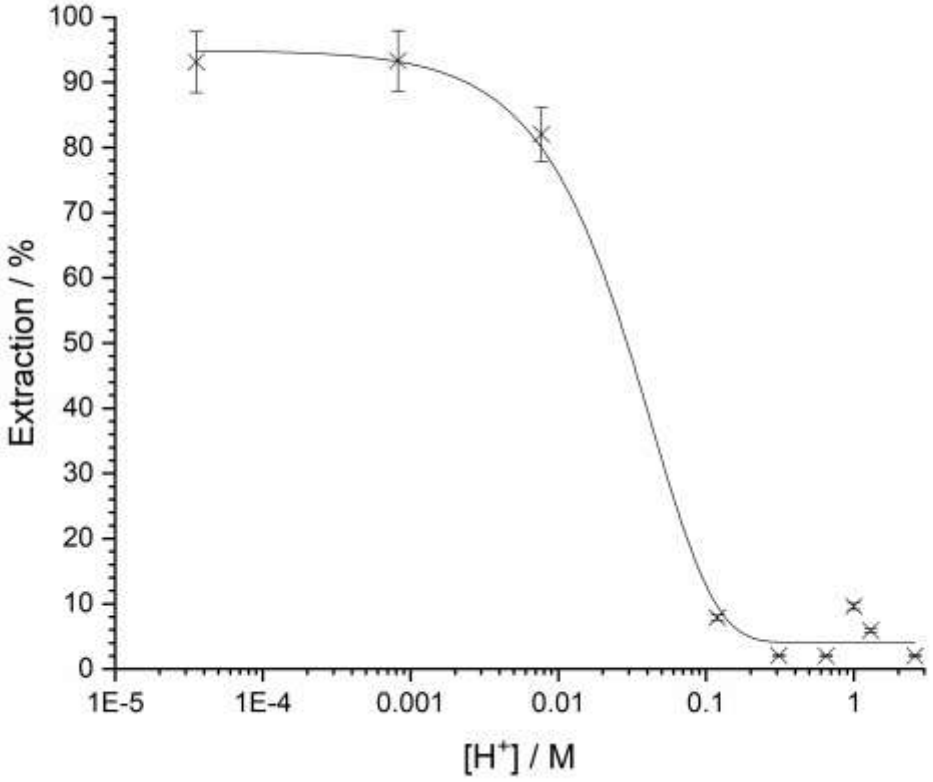

Figure 2. Effect of [H⁺] (HCl) on Cu^{2+} ([Cu^{2+}] = 100 ppm, [H+] = 0.0001 – 1.2 M, T = 30 °C, t = 24 hours) recovery by EBP-Si. Line is to guide the eye only. Error bars are calculated at 5%.

Isotherm loading experiments were performed to assess maximum loading capacity, and models were fit to the collected data. A plot of the collected data does not follow the trend of a traditional isotherm loading curve (Fig. 3). Instead, it appears to be composed of two distinct sections: 0.00 M ≤ C_e ≤ 0.04 M, and C_e ≥ 0.04 M. This implies a change of uptake mechanism. There are multiple potential mechanisms that could be responsible for this, such as ternary complex formation or a change in the number of phosphonic acid groups binding to the Cu^{2+}. However, this is speculative and will require further work using techniques such as X-ray photoelectron spectroscopy (XPS) to fully understand the observed behaviour.

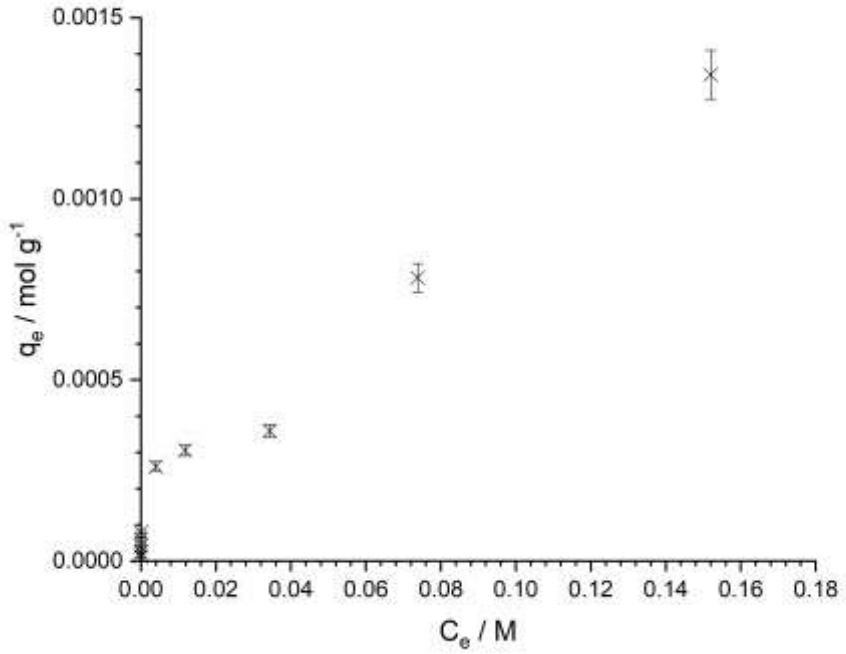

Figure 3. Isotherm plot for Cu^{2+} uptake by EBP-Si (pH = 3, EBP-Si = 8 g, $[Cu^{2+}]_i$ = 25 – 2200 mg L^{-1}, T = 30 °C, t = 24 hours). Error bars are calculated at 5%.

The first section of the plot resembles a traditional isotherm loading curve, and has been fit with the Langmuir (Eq. 2), Dubinin-Radushkevich (Eq. 3), Freundluch (Eq. 4), Tempkin (Eq. 5) and two site Langmuir (Eq. 6) isotherm models; where C_e = $[Cu^{2+}]_{(aq)}$ at equilibrium (M), q_e = $[Cu^{2+}]_{(Si)}$ at equilibrium (mol g^{-1}), q_m = $[Cu^{2+}]_{(Si)}$ maximum (mol g^{-1}), b = Langmuir isotherm constant (L mol^{-1}), B_{DR} = Dubinin-Radushkevich isotherm constant (mol^2 J^{-2}), R = universal gas constant (J mol^{-1} K^{-1}), T = temperature (K), n = Freundlich isotherm adsorption intensity, K_F = Freundlich isotherm constant, A_T = Tempkin isotherm equilibrium binding constant (L g^{-1}), b_T = Tempkin isotherm constant and b_1 and b_2 are Langmuir constants for sites 1 and 2, respectively, in the two-site Langmuir model [25,26]. Fitting parameters for all models are shown in Table 2, with the Dubinin-Radushkevich fit shown in Figure 4.

$$q_e = \frac{q_m b C_e}{1+bC_e} \quad \textbf{(2)}$$

$$q_e = q_m e^{-B_{DR}\left(RTln\left(1+\frac{1}{C_e}\right)\right)^2} \quad \textbf{(3)}$$

$$q_e = K_F C_e^{\frac{1}{n}} \quad \textbf{(4)}$$

$$q_e = \frac{RT}{b_T} ln(A_T C_e) \quad \textbf{(5)}$$

$$q_e = \frac{q_{m1} b_1 C_e}{1 + b_1 C_e} + \frac{q_{m2} b_2 C_e}{1 + b_2 C_e} \quad \textbf{(6)}$$

Table 2. Isotherm model fitting parameters for Cu^{2+} uptake by EBP-Si (pH = 3, EBP-Si = 8 g, [Cu^{2+}] = 25 – 2200 mg L^{-1}). Errors calculated as standard errors at a 99% confidence interval.

	Langmuir	Dubinin-Radushkevich	Freundlich	Tempkin	Two-Site Langmuir
R^2	0.971	0.998	0.973	0.968	0.997
q_m / mol g^{-1}	0.32 ± 0.02	0.47 ± 0.01	-	-	0.36 ± 0.02
q_m / mg g^{-1}	20.46 ± 1.08	29.55 ± 0.57	-	-	22.89 ± 1.27
b / L mol^{-1}	3012 ± 1070	-	-	-	-
B_{DR} / mol^2 J^{-2} ($x10^{-9}$)	-	3.17 ± 0.11	-	-	-
E / kJ mol^{-1}	-	12.55 ± 0.22	-	-	-
K_F ($x10^{-4}$)	-	-	9.45 ± 1.24	-	-
n	-	-	3.76 ± 0.39	-	-
A_T / L g^{-1} ($x10^5$)	-	-	-	1.71 ± 0.62	-
b_T ($x10^7$)	-	-	-	6.51 ± 0.48	-
b_1	-	-	-	-	562.4 ± 217.8
b_2 ($x10^5$)	-	-	-	-	6.99 ± 0.11

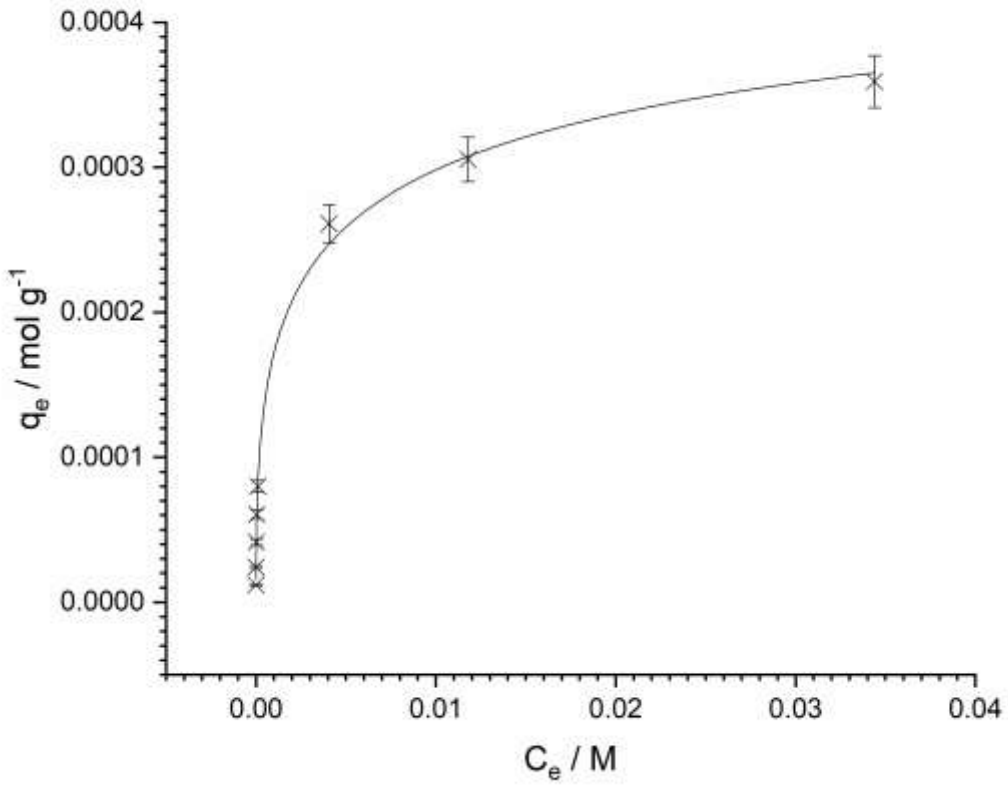

Figure 4. Dubinin-Radushkevich isotherm model fit for Cu^{2+} uptake by EBP-Si for the region 0.00 M ≤ Ce ≤ 0.04 M (pH = 3, EBP-Si = 8 g, [Cu^{2+}] = 25 – 2200 mg L^{-1}, T = 30 °C, t = 24 hours).

The Dubinin-Radushkevich and two-site Langmuir models provide the best fit parameters (R^2) for the collected data. The Dubinin-Radushkevich model is based on sorption to a heterogeneous surface, with a Gaussian energy distribution [18]. As surface modified silica has a heterogeneous surface and the possibility of multiple binding modes for Cu^{2+}, it makes sense that this model fits the best. The two-site Langmuir model also accounts for this heterogeneity as there are two distinct binding sites used to derive the model. The Dubinin-Radushkevich model predicts a q_m value of 29.55 mg g^{-1}; this is higher than the experimentally observed one of 22.82 mg g^{-1}. The prediction by the two-site Langmuir model (22.89 ± 1.27 mg g^{-1}) is much more consistent with the experimental results. A caveat to this model fitting is that we do not know whether the final data point collected in the isotherm experiment exists on the plateau of the isotherm plot, or as part of the second curve at higher [Cu^{2+}] (fig. 3). Therefore conclusions made from model fitting must be treated as tentative, with more study needed to confirm them.

The maximum loading capacity observed for the region 0.00 M ≤ Ce ≤ 0.04 M (22.82 mg g^{-1}, 0.36 mmol g^{-1}) is considered to be relevant, as treated effluents from the HYBRID process will have low [Cu^{2+}]. Additionally, the data does not plateau in the region [Cu^{2+}] > 0.04, so q_m cannot be accurately determined. This is lower than the advertised functionality "labelling" of 0.7 – 1.3 mmol g^{-1} for EBP-Si, potentially meaning that either not all phosphonic acid groups are bound to Cu^{2+}, or that Cu^{2+} may be bound by more than one functionality. This potential 2:1 funtionality:Cu^{2+} ratio also opens the possibility that for $[Cu^{2+}]_{(aq)}$ > 0.04 M, Cu^{2+} sorption moves to a 1:1 binding mode. Table 7 compares Cu^{2+} loading capacity data for published extractants with this work. It is clear that EBP-Si has the lowest q_m out of all extractants referenced, potentially showing that it may not be the most effective extractant. However, it is the only commercially available one in the list, which is important within the context of technology deployability and technology readiness levels (TRL's).

Table 3. Comparison of Cu^{2+} maximum loading capacities and pseudo-second order rate constants for literature extractants.

Functionality	Matrix	q_m / mg g^{-1}	k_2 / g mol^{-1} s^{-1}	Ref
Aminopropyl	Silica gel	66.72*	10.7[a]	[27]
Aminopropyl	Mesoporous silica	25.03*	13.78[b]	[28]
EDTA	Silica	79.37*	2.11[a]	[29]
EDTA	Polystyrene	42.1*	22.57[c]	[30]
Aminomethyl pyridine	Silica gel	49.57	2.82[d]	[31]
Phosphonic acid	Silica	22.82	213.996[a]	This work

*Maximum loading capacities from isotherm fitting models, not the experimentally measured value; [a]measured at 30 °C, [b]measured at room temperature, [c]measured at 20 °C, [d]measured at 25 °C.

The mean free energy of sorption was calculated from derived parameters from the Dubinin-Radushkevich isotherm model (Eq. 6). The mean energy of sorption (E) was determined to be 12.55 kJ mol^{-1}, a value that corresponds to a chemical ion exchange interaction, as opposed to a physisorption interaction. E values derived from Dubinin-Radushkevich fits of Co^{2+} and Ni^{2+} loading onto EBP-Si are lower than for Cu^{2+} (7.65 and 7.23 kJ mol^{-1}, respectively) [18]. This suggests a stronger binding interaction between the functionality and Cu^{2+} than with Co^{2+} and Ni^{2+}, which has implications for the mixed metal loading experiments discussed below. A caveat to this is that in the previous work where the E values for Co^{2+} and Ni^{2+} were derived, all other collected data pointed to chemically, as opposed to a physically, bound species. This highlights the inaccuracies associated with using isotherm models when the exact extraction mechanism is unknown, although this does not detract from their usefulness for comparative studies and in moving towards true mechanistic understanding.

$$E = \frac{1}{\sqrt{2B_{DR}}} \quad \textbf{(6)}$$

3.2. Kinetic Loading Studies

Uptake kinetics experiments were performed at T = 30, 40, 50 and 60 °C. Rapid extraction was observed, with equilibrium being reached within 10 minutes of contact time. Data were fit to the pseudo-first (Eq. 7) and pseudo-second (Eq. 8) order rate equations; where $q_t = [Cu^{2+}]_{(Si)}$ at time t (mol g^{-1}), $q_e = [Cu^{2+}]_{(Si)}$ at equilibrium (mol g^{-1}), k_1 = pseudo-first order rate constant (g mol^{-1} s^{-1}), k_2 = pseudo-second order rate constant (g mol^{-1} s^{-1}), and t = time (s). Fitting data is given in Table 4, and model fits are shown in Figure 5.

$$q_t = q_e(1 - e^{-k_1 t}) \quad \textbf{(7)}$$

$$q_t = \frac{k_2 q_e^2 t}{1 + k_2 q_e t} \quad \textbf{(8)}$$

Determined rate constants for Cu^{2+} extraction by EBP-Si are significantly higher (up to 2 orders of magnitude) than those found in the literature (Table 3). One reason for these rapid kinetics is that EBP-Si is not porous, so there are no rate determining factors related to particle diffusion. This suggests that the rate determining step is the adsorption process itself, the binding of Cu^{2+} to the phosphonic acid moiety, which accounts for the pseudo-second order kinetic model showing a superior fit over the other models used. The same behaviour has been seen before with EBP-Si when extracting Co^{2+} and Ni^{2+} from aqueous media [18]. This theory was checked through the subsequent fitting of film diffusion, particle diffusion and Elovich kinetic models, where adequate goodness of fit values were not obtained (Table 5). Results are also consistent with the isotherm model fitting, building a picture of a chemically bound Cu^{2+} with a strong interaction between the phosphonic acid moiety and the Cu^{2+} ion.

Table 4. Fitting parameters for the pseudo-first and -second order kinetic models for uptake of Cu^{2+} by EBP-Si. Errors calculated as standard errors at a 99% confidence interval.

T / °C	R^2		q_e / mol g^{-1} (x10^{-4})	k_2 / g mol^{-1} s^{-1}
	1st order	2nd order		
30	0.748	0.999	2.138 ± 0.019	213.996 ± 3.664
40	0.391	0.999	2.082 ± 0.036	366.605 ± 12.237
50	0.091	0.999	2.061 ± 0.043	764.716 ± 30.502
60	0.486	0.992	1.921 ± 0.090	1064.622 ± 96.366

Table 5. R^2 values for the fitting of kinetic data to film diffusion, particle diffusion and Elovich models.

T / °C	R^2		
	Film Diffusion	**Particle Diffusion**	**Elovich**
30	0.4665	0.6610	0.8364
40	0.4876	0.6644	0.8275

50	0.3220	0.4742	0.6743
60	0.0017	0.5852	0.6980

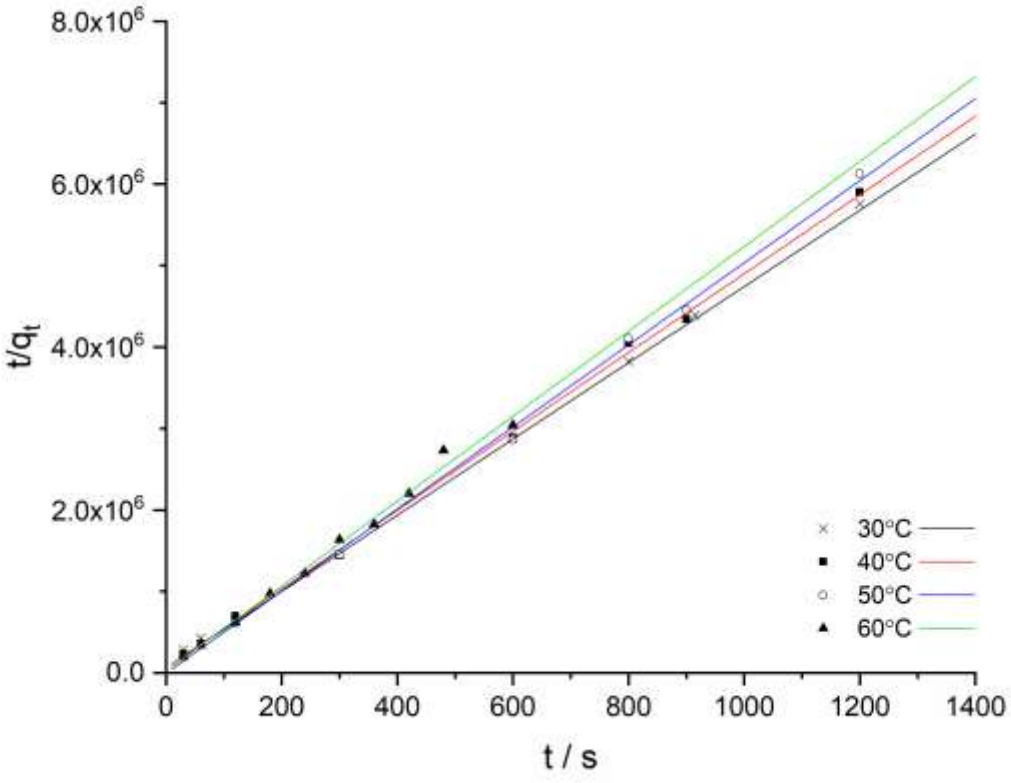

Figure 5. Pseudo-second order kinetic model fits for Cu^{2+} uptake by EBP-Si with varying temperature (pH = 3, EBP-Si = 0.8 g, [Cu^{2+}] = 100 mg L^{-1}).

Rate constants derived from the pseudo-second order kinetic model were used to determine thermodynamic data using the Eyring (Eq. 9) and Arrhenius (Eq. 10) equations; where k_2 = 2nd order rate constant (g mol^{-1} s^{-1}), T = temperature (K), k_B = Boltzmann constant (m^2 kg s^{-2} K^{-1}), h = Planck constant, $\Delta S^{\#}$ = entropy of activation (J K^{-1}), $\Delta H^{\#}$ = enthalpy of activation (J mol^{-1}), R = universal gas constant, A = pre-exponential factor and E_A = active activation energy (J mol^{-1}) [32,33]. It then follows that the Gibbs free energy of activation ($\Delta G^{\#}$, J mol^{-1}) can be calculated using Equation 11. The resulting Eyring and Arrhenius plots are shown in Figure 6, and fitting parameters for both are shown in Table 6.

$$\frac{ln(k_2)}{T} = \left(\frac{ln(k_b)}{h} + \frac{\Delta S^{\#}}{R}\right) - \frac{\Delta H^{\#}}{RT} \quad \textbf{(9)}$$

$$ln(k_2) = ln(A) - \frac{E_A}{RT} \quad \textbf{(10)}$$

$$\Delta G^{\#} = \Delta H^{\#} - T\Delta S^{\#} \quad \textbf{(11)}$$

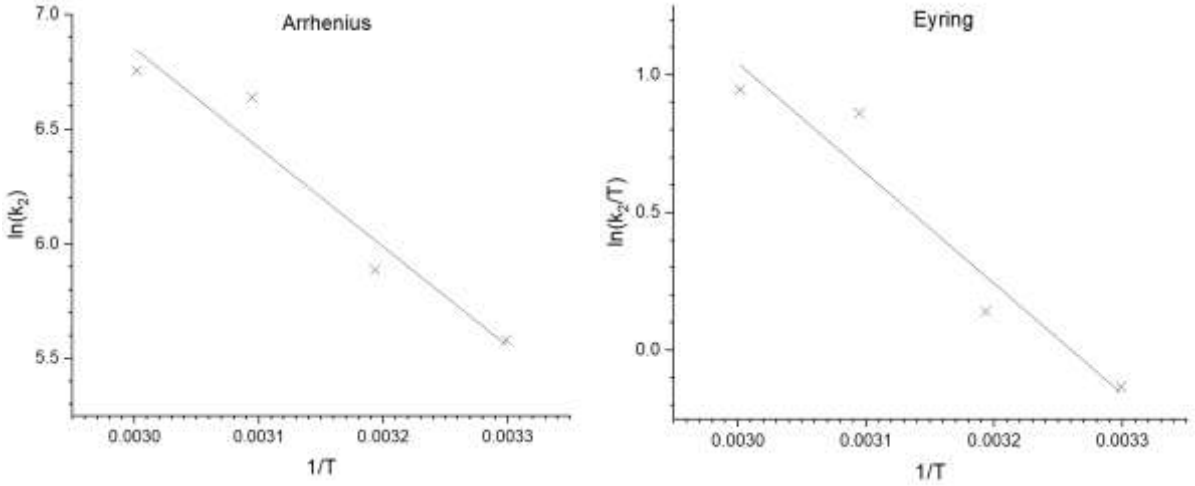

Figure 6. Arrhenius plot (left, y = -4324.902x + 19.826, R^2 = 0.935) and Eyring plot (right, y = -4007.307x + 13.065, R^2 = 0.925) for uptake of Cu^{2+} by EBP-Si ([Cu^{2+}] = 100 ppm, pH = 3, t = 30, 40, 50 and 60 °C).

Table 6. Thermodynamic values derived from Eyring and Arrhenius plots of Cu^{2+} uptake by EBP-Si.

A (x10^{10})		2.348 ± 0.150
E_a / kJ mol^{-1}		46.653 ± 4.032
$\Delta H^{\#}$ / kJ mol^{-1}		-44.013 ± 4.043
$\Delta S^{\#}$ / J K^{-1}		-55.219 ± -4.940
$\Delta G^{\#}$ / kJ mol^{-1}	**30 °C**	-27.273 ± 4.311
	40 °C	-26.721 ± 4.329
	50 °C	-26.169 ± 4.347
	60 °C	-25.617 ± 4.365

The thermodynamic parameters extracted from the Arrhenius and Eyring plots show that Cu^{2+} sorption is spontaneous and enthalpically favourable. The negative $\Delta S^{\#}$ value shows that there is an ordered Cu^{2+} coordination environment when it is bound to EBP-Si. This is consistent with the mean free energy of sorption derived from the Dubinin-Radushkevich isotherm model fit. Both the $\Delta H^{\#}$ and $\Delta G^{\#}$ values show that Cu^{2+} sorption by EBP-Si is an exothermic process. This agrees with work by Kumar *et. al.* for Cu^{2+} sorption by surface modified agricultural waste [34], however, there are reports positive $\Delta H^{\#}$ and $\Delta G^{\#}$ values in the literature [35–37]. The $\Delta G^{\#}$ values calculated by Kumar *et. al.* are smaller than those reported here, which makes sense as they report the rate limiting step to be diffusion controlled, as opposed to surface complexation controlled.

3.3. Column Loading Studies

Breakthrough curves for dynamic uptake of Cu^{2+} by EBP-Si at varying flow rate (2.75, 11.00 and 22.00 BV hr^{-1}) are shown in Figure 7. Little dependence of Cu^{2+} recovery on flowrate can be seen, with sharp breakthrough curves for all studied flowrates. This is indicative of fast kinetics, agreeing

with the batch kinetic studies and literature data for Co^{2+} and Ni^{2+} recovery by EBP-Si [18]. Breakthrough data has been fit with the modified dose response (MDR) (Eq. 12),
Thomas (Eq. 13) and Yoon-Nelson (Eq. 14) models; where C = $[Cu^{2+}]_{effluent}$ (M), C_i = $[Cu^{2+}]_{influent}$ (M), a = MDR constant, b = MDR constant, V_{ef} = effluent volume (mL), t = time (min), N_0 = saturation capacity (mg L^{-1}), K_{YN} = Yoon-Nelson constant (min^{-1}), t_{50} = time to 50% column saturation (min), K_{TH} = Thomas constant (L mg^{-1} min^{-1}), m = mass of EBP-Si (g), Q = flowrate (mL min^{-1}) and q_m = saturation capacity (mg g^{-1}) [38]. Fitting parameters are shown in Table 7.

$$\frac{C}{C_i} = 1 - \frac{1}{1+\left(\frac{V_{ef}}{b}\right)^a} \quad \textbf{(12)}$$

$$\frac{C}{C_i} = \frac{1}{1+e^{\left(\frac{K_{TH}}{Q}\right)\left(q_m m - C_i V_{eff}\right)}} \quad \textbf{(13)}$$

$$\frac{C}{C_i} = \frac{1}{1+e^{K_{YN}(t_{50}-t)}} \quad \textbf{(14)}$$

Table 7. Fitting parameters for the modified dose response, Yoon-Nelson and Thomas models for the column loading of Cu^{2+} onto EBP-Si.

	2.75 BV hr^{-1}		
	MDR	**YN**	**T**
R^2	0.99604	0.99459	0.99459
q_m / mg g^{-1}	14.674 ± 0.185	-	10.72 ± 0.0157
a	23.759 ± 0.668	-	-
b	83.551 ± 0.105	-	-
t_{50} / min	-	1520.481 ± 8.236	-
K_{YN} / min^{-1}	-	0.018 ± 5.403E-4	-
K_{TH} / L mg^{-1} min^{-1}	-	-	0.184 ± 0.006
	11 BV hr-1		
	MDR	**YN**	**T**
R^2	0.99931	0.99888	0.99888
q_m / mg g^{-1}	14.262 ± 0.206	-	10.424 ± 0.019
a	21.783 ± 0.634	-	-
b	81.204 ± 0.117	-	-
t_{50} / min	-	354.942 ± 1.892	-
K_{YN} / min^{-1}	-	0.070 ± 0.002	-
K_{TH} / L mg^{-1} min^{-1}	-	-	0.695 ± 0.026
	22 BV hr-1		
	MDR	**YN**	**T**
R^2	0.99784	0.99796	0.99796
q_m / mg g^{-1}	13.605 ± 0.490	-	9.963 ± 0.035
a	15.671 ± 0.777	-	-
b	77.463 ± 0.279	-	-
t_{50} / min	-	173.409 ± 1.540	-

K_{YN} / min^{-1}	-	0.103 ± 0.005	-
K_{TH} / L mg^{-1} min^{-1}	-	-	1.029 ± 0.049

Surprisingly, all of the fitting models, though based on different theoretical assumptions, fit the collected data adequately. Again, this demonstrates potential problems with "generic" models, as opposed to more accurate ones derived from the underlying mechanism of extraction. Generally, the MDR model gives a slightly better fit than the others do, but the difference is so small as to be considered negligible. Derived q_m values are higher from the MDR than the Thomas model, however, they are relatively consistent between flowrates. Again, this agrees with the current theory that EBP-Si exhibits rapid uptake kinetics.

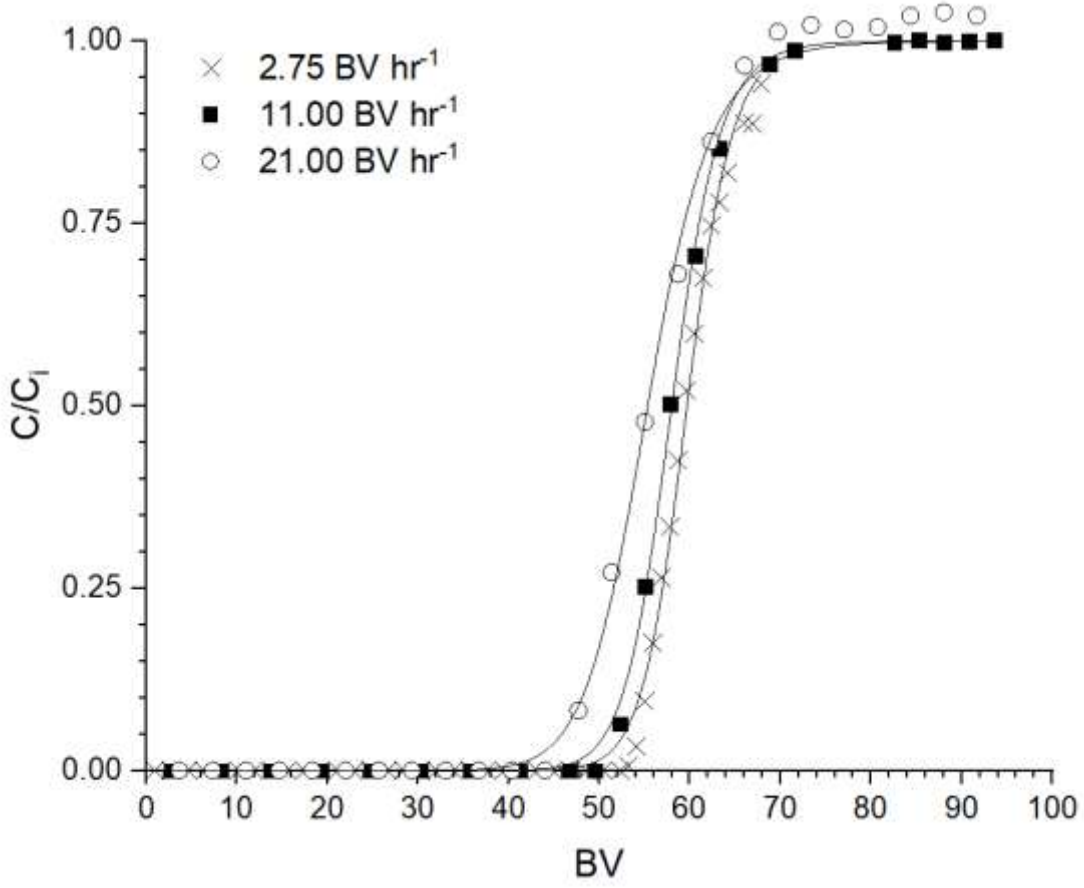

Figure 7. Breakthrough curves for Cu^{2+} loading on EBP-Si and varying flowrate (pH = 3, [Cu^{2+}] = 0.1 g L^{-1}, T = room temperature). Data fitted with the Modified Dose Response model.

Derived q_m values are all lower then than that determined in the isotherm studies, suggesting that the change in mechanism is not important for these dynamic experiments. This will be due to the influent [Cu^{2+}] (0.1 g L^{-1}, 1.6 mM) being below the concentration where the change in mechanism occurs.

Further column studies were performed with solutions containing Co^{2+} and Ni^{2+} in addition to Cu^{2+}. High flowrates were chosen due to the observed fast uptake kinetics (69, 138 and 206 BV hr^{-1}). Breakthrough curves are shown in Figure 8. Cu^{2+} has the highest affinity for EBP-Si at all flowrates tested. The behaviour of Co^{2+} and Ni^{2+} is more complicated, however, the general trend in affinity over the full range of flowrates tested is Cu^{2+} > Co^{2+} > Ni^{2+}. Onset of Cu^{2+} breakthrough happens earlier as you move from slower to faster flowrates.

The observed affinity trend is consistent with E values derived from the Dubinin-Radushkevich isotherm (12.11, 7.65 and 7.23 kJ mol^{-1}, respectively, for Cu^{2+}, Co^{2+} and Ni^{2+}) [18]. Not only do these values predict the affinity order in the studied dynamic system, they also predict the similarity in Co^{2+} and Ni^{2+} breakthrough volumes. The observed trend is relatively consistent with stability constants for the studied metals binding with ethylphosphonic acid (logK = 3.60, 2.27 and 2.30 kJ mol^{-1}, respectively, for Cu^{2+}, Co^{2+} and Ni^{2+}) [39]. The values for Co^{2+} and Ni^{2+} are almost the same (and actually reversed to the observed trend), which suggests that there may be another factor effecting the affinity. It must be noted, however, that these stability constants relate to aqueous phase complexes, which will be different to those for metal binding to a functionalised surface. An important factor to consider is water exchange kinetics, as there is likely to be dehydration of the metal centre when in proximity to the silica surface. More labile metals should exhibit faster exchange kinetics, which is indeed the case (Eq. 15 and 16) [39]. The more rapid exchange kinetics for Co^{2+} explains the affinity order, with the kinetics being more important than thermodynamics for explaining the observed $Co^{2+} > Ni^{2+}$ affinity order.

$$[Co(H_2O)_5Cl]^+ + \mathbf{H_2O} \rightarrow [Co(H_2O)_5(\mathbf{H_2O})Cl]^+ + H_2O \qquad \log k = 7.23 \qquad \textbf{(15)}$$

$$[Ni(H_2O)_5Cl]^+ + \mathbf{H_2O} \rightarrow [Ni(H_2O)_5(\mathbf{H_2O})Cl]^+ + H_2O \qquad \log k = 5.15 \qquad \textbf{(16)}$$

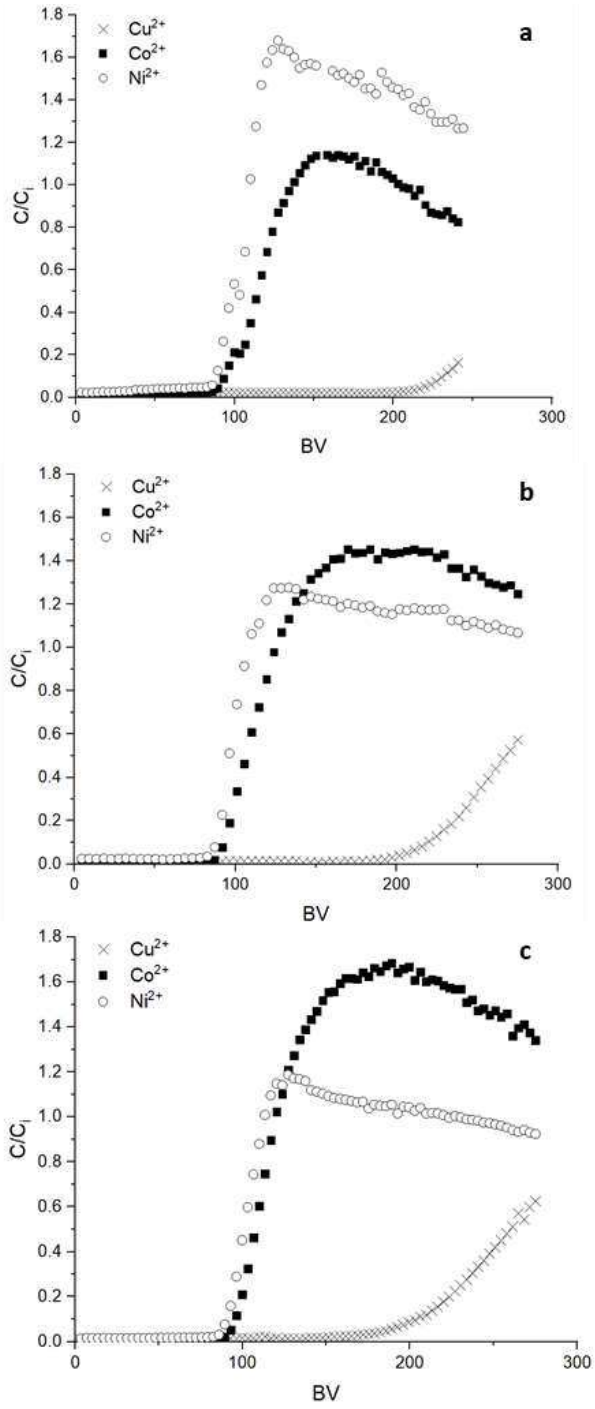

Figure 8. Breakthrough curves for a Cu^{2+}, Co^{2+}, Ni^{2+}on EBP-Si from a mixed metal solution (pH = 3, $[M]_{total}$ = 0.1 g L^{-1}, $[Cu^{2+}] = [Co^{2+}] = [Ni^{2+}]$, T = room temperature) at 69 BV hr^{-1} (a), 138 BV hr^{-1} (b) and 206 BV hr^{-1} (c)

This affinity trend does not agree with what has been seen for the phosphonic acid functionalized resin Duolite C-63 [40]. The observed affinity for a set of metals to the resin (in the hydrogen form) was determined to be $Mg^{2+} > Co^{2+} \sim Ni^{2+} > Ca^{2+} > Cu^{2+}$. Interestingly, this trend was not seen when the resin was in the sodium form, with no discernible difference between affinities for each metal. However, work by Yamabe *et. al.* describes an affinity series for a phosphonic acid functionalized polystyrene resin which does agree with the data collected in this paper ($Pb^{2+} > Mn^{2+} > \approx Cd^{2+} \approx Cu^{2+} > Ca^{2+} \approx Co^{2+} \approx Zn^{2+} \approx Ba^{2+} \approx Sr^{2+} > Ni^{2+} \approx Mg^{2+}$) [41]. Differences in the affinity series can largely be put down to experimental method, the work with Duolite C-63 utilised pH buffers, whereas this work and

the work by Yamabe *et. al.* did not. The buffer used was a mixture of acetic acid and sodium acetate. Acetate (Ac) is known to bind with Cu^{2+}, Co^{2+} and Ni^{2+}, which will affect the uptake equilibrium. Interestingly, out of those three metals, Ac binds most strongly with Cu^{2+}, forming complexes with 1, 2 or 3 ligands, with logK values of 1.67, 2.69 and 3.0, respectively [39]. Co^{2+} and Ni^{2+} both make complexes with 1 or 2 Ac ligands, with logK values of 0.81, 0.8, 0.76 and 1.27, respectively for $CoAc_1$, $CoAc_2$, $NiAc_1$ and $NiAc_2$, respectively.

4. Conclusions

The extraction behaviour of Cu^{2+} by EBP-Si has been determined in both batch and column loading systems, as well as its competition behaviour with Co^{2+} and Ni^{2+} in a column loading system. Increasing acidity below pH 3 has been shown to have a negative effect on Cu^{2+} loading, causing uptake suppression.

Isotherm loading studies suggested that there are two different Cu^{2+} extraction mechanisms, with a transition from one to the other at high $[Cu^{2+}]_{(aq)}$ (> 0.04 M). The maximum loading capacity at process relevant $[Cu^{2+}]$ was experimentally determined to be 22.82 mg g^{-1}. Isotherm models were fit to the collected data, with the highest R^2 value being found for the Dubinin-Radushkevich model (0.998). The maximum Cu^{2+} loading capacity is lower than that seen for many adsorbents in the literature, though this negative is believed to be outweighed by the positive kinetic behaviour observed, as well as its potential to be converted directly into a nuclear waste glass of concrete.

EBP-Si was observed to have rapid kinetics, with all Cu^{2+} being removed from solution within 10 minutes under the tested experimental conditions. Data was fit to multiple kinetic models, with the pseudo-second order model giving the best R^2 value. All models based on diffusion controlled kinetics gave poor goodness of fit values, thus leading to the conclusion that the chemical binding of Cu^{2+} to the phosphonic acid moiety via ion exchange is the rate determining step. Additionally, 2^{nd} order rate constants were much higher than those found in the literature for Cu^{2+} extraction, generally by one or two orders of magnitude.

Column loading studies were consistent with the kinetic studies, showing sharp breakthough profiles in individual Cu^{2+} loading systems. Cu^{2+} outcompetes Co^{2+} and Ni^{2+} for extraction by EBP-Si under dynamic loading conditions, with the affinity order being $Cu^{2+} > Co^{2+} > Ni^{2+}$. This order can be understood using stability constants for the metal ions with ethylphosphonic acid and water exchange kinetics.

The collected data in this paper show that the Cu^{2+} present in effluents generated in the HYBRID process will have a profound impact on the use of EBP-Si for their decontamination. The ability of Cu^{2+} to eject Co^{2+} from the extractant is particularly worrying, as ^{60}Co is an important radioactive contaminant in decommissioning effluents. If EBP-Si is to be used as a “direct to wasteform” extractant then the Cu^{2+} will need to be removed from the effluent before it passes through the EBP-Si column (Figure 9). This is easily possible through the use of a copper selective ion exchange resin, such as the isothiouronium functionalised resin Purolite MTS9200.

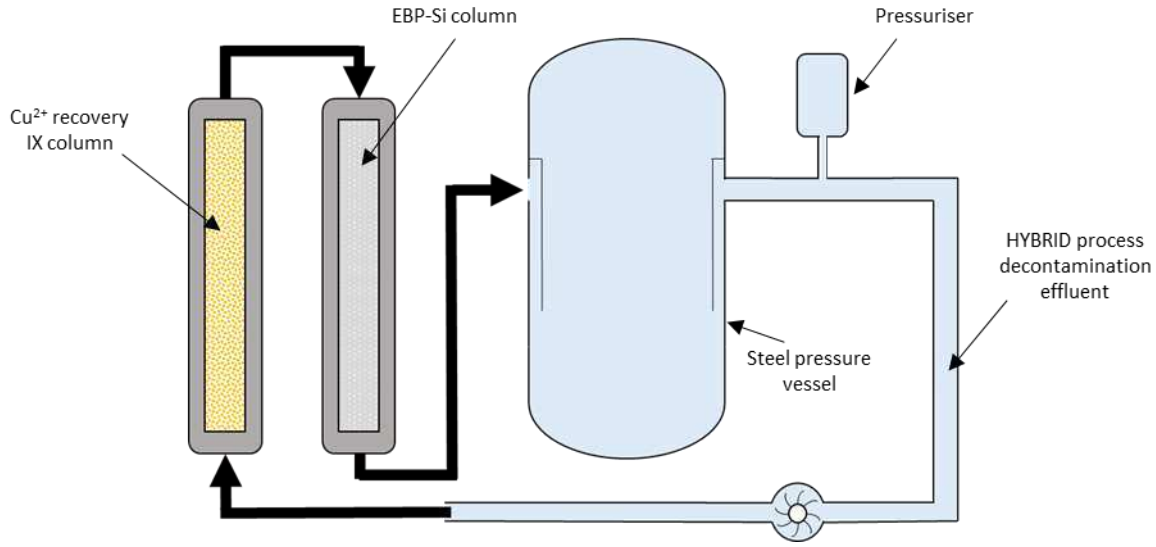

Figure 9. Schematic of proposed primary coolant loop decontamination process using EBP-Si.

5. Acknowledgements

The authors would like to thank the members of the SNUCER group at the University of Sheffield for their help in facilitating the success of this work.

6. Funding

This work was funded by the UK Engineering and Physical Sciences Research Council through the Doctoral Prize Fellowship and the UK Korea Civil Nuclear Energy program grant EP/M026558/1 Silicate Nanoparticles for extraction of Radionuclides (SINNER)

7. References

[1] IAEA, Energy, Electricity and Nuclear Power Estimates for the Period up to 2050, Vienna, 2018.
[2] J.B. Chung, E.S. Kim, Energy Policy 116(January) (2018) 137–44. 10.1016/j.enpol.2018.02.007.
[3] V. Nian, Prog. Nucl. Energy 105(December 2017) (2018) 83–98.
[4] H.W. Seo,, W. Sohn,, K.H. Jo, Ann. Nucl. Energy 120 (2018) 749–62.
[5] K.W. Kim, M.J. Kim, M.K. Oh, J. Kim, H.H. Sung, R.I. Foster, K.-Y. Lee, J. Nucl. Sci. Technol. 00(00) (2018) 1–14.
[6] A.J. Canner, S.E. Pepper, M. Hayer, M.D. Ogden, Prog. Nucl. Energy 104(October 2017) (2018) 271–9.
[7] J.Y. Jung, S.Y. Park, H.J. Won, S.B. Kim, W.K. Choi, J.K. Moon, S.J. Park, Met. Mater. Int. 21(4) (2015) 678–85.
[8] R. Morris, Water Chemistry of Nuclear Reactor Systems 8, ICE Publishing, Bournemouth, UK, 2000, pp. 452–4.
[9] W.K. Choi, H.J. Won, S.Y. Park, S.B. Kim, J.Y. Jung, J.K. Moon, Waste Management 2015, Pheonix, Arizona, US, 2015, p. .
[10] H.J. Won, J.S. Park, C.H. Jung, S.Y. Park, W.K. Choi, J.K. Moon, Proceedings of the ASME 2013 15th International Conference on Environmental Remediation and Radioactive Waste

Management, Brussels, Belgium, 2018, p. .
[11] H.J. Won, W.S. Lee, C.H. Jung, S.Y. Park, W.K. Choi, Moon, Asian J. Chem. 26(5) (2015) 1327–30.
[12] G.J. Lumetta, K.L. Nash, S.B. Clark, J.I. Friese, Separations for the Nuclear Fuel Cycle in the 21st Century, American Chemical Society, 2006.
[13] J. Veliscek-Carolan, J. Hazard. Mater. 318 (2016) 266–81.
[14] J.T.M. Amphlett, C.A. Sharrad, M.D. Ogden, Chem. Eng. J. 342 (2018) 133–41.
[15] E.M. Moon, M.D. Ogden, C.S. Griffith, A. Wilson, J.P. Mata, J. Ind. Eng. Chem. 51 (2017) 255–63.
[16] N. Akhtar, J. Iqbal, M. Iqbal, Eng. Life Sci. 4(2) (2004) 171–8.
[17] M.G. Mahfouz, A.A. Galhoum, N.A. Gomaa, S.S. Abdel-Rehem, A.A. Atia, T. Vincent, E. Guibal, Chem. Eng. J. 262 (2015) 198–209.
[18] S.E. Pepper, K.R. Whittle, L.M. Harwood, J. Cowell, S. Lee, M.D. Ogden, S.E. Pepper, K.R. Whittle, L.M. Harwood, J. Cowell, T.S. Lee, Cobalt, Sep. Sci. Technol. 53(04) (2017) 1–11.
[19] R. Hanzel, P. Rajec, J. Radioanal. Nucl. Chem. 246(3) (2000) 607–15.
[20] T. Gholami, M. Salavati-niasari, M. Bazarganipour, Superlattices Microstruct. 61 (2013) 33–41.
[21] F. Xie, X. Lin, X. Wu, Z. Xie, Talanta 74 (2008) 836–43.
[22] J.T.M. Amphlett, M.D. Ogden, R.I. Foster, N. Syna, K. Soldenhoff, C.A. Sharrad, Chem. Eng. J. (2018).
[23] H.P. Gregor, M. Taiferi, L. Citarel, E.I. Becker, Ind. Eng. Chem. 44(12) (1952) 2834–9.
[24] O. Abderrahim, M.A. Didi, D. Villemin, J. Radioanal. Nucl. Chem. 279(1) (2009) 237–44.
[25] K.Y. Foo, B.H. Hameed, Chem. Eng. J. 156(1) (2010) 2–10.
[26] J. Koresh, A. Soffer, J. Colloid Interface Sci. 92(2) (1983) 517–24.
[27] V. Manu, H.M. Mody, H.C. Bajaj, R. V. Jasra, Ind. Eng. Chem. Res. 48(19) (2009) 8954–60.
[28] H. Yang, R. Xu, X. Xue, F. Li, G. Li, J. Hazard. Mater. 152(2) (2008) 690–8.
[29] R. Kumar, M.A. Barakat, Y.A. Daza, H.L. Woodcock, J.N. Kuhn, J. Colloid Interface Sci. 408(1) (2013) 200–5.
[30] L. Wang, L. Yang, Y. Li, Y. Zhang, X. Ma, Z. Ye, Chem. Eng. J. 163(3) (2010) 364–72.
[31] L. Bai, H. Hu, W. Zhang, J. Fu, Z. Lu, M. Liu, H. Jiang, L. Zhang, Q. Chen, P. Tan, J. Mater. Chem. 22(33) (2012) 17293–301.
[32] M. Mohapatra, S. Khatun, S. Anand, Chem. Eng. J. 155(1–2) (2009) 184–90.
[33] H. Li, J. Li, Z. Chi, W. Ke, Procedia Environ. Sci. 16(Iii) (2012) 646–55.
[34] P. Senthil Kumar, C. Senthamarai, A. Durgadevi, Environ. Prog. Sustain. Energy 33(1) (2014) 28–37.
[35] M. El-Batouti, O.M. Sadek, F.F. Assaad, J. Colloid Interface Sci. 259(2) (2003) 223–7.
[36] L. Dong, L. Yanyan, Y. Junxia, D. Yigang, J. Dispers. Sci. Technol. 38(2) (2017) 180–6.
[37] L. Ćurković, M. Trgo, M. Rožić, N.V. Medvidović, Indian J. Chem. Technol. 18(2) (2011) 137–44.
[38] J.T.M. Amphlett,, C.A. Sharrad,, R.I. Foster,, M.D. Ogden, J. South African Inst. Min. Metall. 12 (2018) 1251–7.
[39] R.M. Smith, A.E. Martell, R.J. Motekaitis, NIST Standard Reference Database 46, Gaithersburg, MD, 2004.
[40] A.K. Mukherji, Zeitschrift Fur Anal. Chemie 226(5) (1966) 401–5.
[41] T. Ihara, A. Jyo, K. Yamabe, Sep. Sci. Technol. 36(15) (2001) 3511–28.